Stochastic estimation of hydraulic transmissivity fields using flow connectivity indicator data

G. Freixas, D. Fernàndez-Garcia and X. Sanchez-Vila

Hydrogeology Group (UPC-CSIC), Department of Civil and Environmental Engineering, Universitat Politècnica de Catalunya (UPC), Jordi Girona 1-3, 08034 Barcelona, Spain.

Abstract

Most methods for hydraulic test interpretation rely on a number of simplified assumptions regarding the homogeneity and isotropy of the underlying porous media. This way, the actual heterogeneity of any natural parameter, such as transmissivity (T), is transferred to the corresponding estimates in a way heavily dependent on the interpretation method used. An example is a long-term pumping test interpreted by means of the Cooper-Jacob method, which implicitly assumes a homogeneous isotropic confined aquifer. The estimates obtained from this method are not local values, but still have a clear physical meaning; the estimated T represents a regional-scale effective value, while the log-ratio of the normalized estimated storage coefficient, indicated by w', is an indicator of flow connectivity, representative of the scale given by the distance between the pumping and the observation wells. In this work we propose a methodology to use w', together with sampled local measurements of transmissivity at selected points, to map the expected value of local T values using a technique based on cokriging. Since the interpolation involves two variables measured at different support scales, a critical point is the estimation of the covariance and crosscovariance matrices. The method is applied to a synthetic field displaying statistical anisotropy, showing that the inclusion of connectivity indicators in the estimation method provide maps that effectively display preferential flow pathways, with direct consequences in solute transport.

Keywords: flow connectivity indicator, Cooper-Jacob method, transmissivity, parameter estimation, anisotropy, cokriging.

Highlights:

- Cooper-Jacob estimates of storage coefficient, as indicators of flow connectivity, are spatial integrals of local transmissivities
- Estimates of S can be used to map expected local transmissivities through cokriging
- Statistical anisotropy and the presence of conducting features can be reconstructed from this method

1. Introduction

Hydraulic connectivity between two points is quite a well defined concept in fractured media [e.g., *Neuman*, 2008], but a loosely defined concept in porous media [e.g., *Knudby and Carrera*, 2005]. While in the latter case a formal definition is not available, point-to-point connectivity is considered directly linked to the inherent heterogeneity of natural porous media [*Trinchero et al.*, 2008]. The issue of flow connectivity has been a concern to the scientific community from the past years, with the first studies in the field of oil engineering. *Fogg* [1986] was the first to launch the concept of flow connectivity in a study of a detailed 3D model of the Wilcox aquifer in Texas. He showed that the flow occurring in a sedimentary aquifer is determined to a greater extent by the connectivity of the medium as compared to the local values of hydraulic conductivity. Thereafter the term connectivity was extended to transport of conservative species [*Poeter and Townsend*, 1994] by looking at the spatial distribution of travel times in an alluvial aquifer.

Hydraulic connectivity concepts are widely present implicitly in the literature. *Schad and Teutsch* [1994] analysed the time drawdown curves in tests performed at different scales and found that natural heterogeneity reflected on the hydraulic parameters estimated from field tests, indicating that pumping tests could be a good tool to map heterogeneity. *Sanchez-Vila et al.* [1996] discussed the presence of scale effects in transmissivity through numerical simulations, and provided a justification for the non-log-normality of the multivariate statistics in real fields; they found that an asymmetry in the multivariate distribution of local T values, i.e., connectivity between zones of high transmissivity being larger than those of low transmissivity, resulted in effective transmissivity (T_{eff}) values higher than the geometric mean of point T values. *Schulze-Makuch and Cherkauer* [1998] demonstrated through aquifer tests and numerical simulations in a porous carbonate aquifer that the estimated hydraulic conductivity increased with the duration of the tests, linked to the increase in the volume of aquifer impacted. *Attinger* [2003] used a coarse graining method to upscale the flow equation in heterogeneous media and found that connectivity had a clear impact in the resulting piezometric head distribution. *Zinn and Harvey* [2003] described the upscaled flow (and also transport) characteristics of three synthetic hydraulic conductivity fields selected to have the same pdfs of local conductivity values and very similar variograms, but with

different degrees of connectivity, finding its impact on effective transmissivity and travel times. Finally, *Zhou et al.* [2011] applied the Ensemble Kalman Filter method to generate realizations that directly embedded the connectivity of conductivity fields.

While in this work we deal with connectivity in porous structures, in the literature a number of works define it in fractured media, where it is mostly associated to the presence of connected fracture networks. The most widely used approach involves the description of such networks from power law length distributions in discrete fracture models and the implication upon flow patterns [e.g., *Bour and Davy*, 1997; *Odling*, 1997; *Guimerà and Carrera*, 2000; *Ji et al.*, 2011; *Xu et al.*, 2006]. Further, *De Marsily et al.* [2005] presented a review of continuous Geostatistical, Boolean, Indicator or Gaussian-Threshold models in order to address rock strata connectivity, incorporating geologic information. Additional work has been performed in the framework of discrete fracture models; an example is the study of *Neuman* [2008], developing a methodology relating fracture type and corresponding fractal attributes. In terms of connectivity, one of the most significant points of that study is establishing a relationship between permeability, scale length of fractures, and average fracture apertures.

Regarding the definition of hydraulic connectivity as a quantifiable parameter, *Renard and Allard* [2013] provided a classification distinguishing static and dynamic metrics. According to these authors, the static connectivity metrics are only a function of the spatial distribution of lithology and permeability, while the dynamic metrics represent better the physics but they depend on geometrical and physical parameters, such as the type of boundary conditions or the state of the system. Along this classification, static metrics, include the works of *Deutsch* [1998] who analyse 3D connectivity numerical models, *Vogel and Roth* [2001] who determined a connectivity function based on pore-network models, *Pardo-Igúzquiza and Dowd* [2003] who created a code that performed an analysis based on a number of connectivity statistics. Moreover, *Knudby et al.* [2006] presented a binary upscaling formula incorporating connectivity information, *Western et al.* [2001] assigned connectivity functions (from Boolean models) to synthetic aquifer conductivity patterns, *Schlüter and Vogel* [2011] analysed the potential of various morphological descriptors sensitive to structural connectivity patterns based on percolation theory to predict flow and transport in heterogeneous porous media, and *Neuweiler et al.* [2011] estimated the effective parameters for an upscaled model for a

buoyant counter flow of DNAPL and water in a closed box filled with heterogeneous porous material.

On the other hand, dynamic connectivity metrics are more related to our work, and imply another type of indicators. The reference works that form the basis of our analysis are those of *Meier et al.* [1998] and *Sanchez-Vila et al.* [1999]. These authors studied the information that is embedded in the traditional estimates of transmissivity (T_{est}) and storage coefficient (S_{est}) when data from a long-term pumping test performed under constant flow rate was interpreted using the traditional Cooper-Jacob [*Cooper and Jacob*, 1946] approach based on the development of a linear response of drawdown vs log time curve. The combination of the numerical analysis of *Meier et al.* [1998] with the analytical work of *Sanchez-Vila et al.* [1999] indicated that S_{est} incorporated information about the hydraulic connectivity between the pumping and the observation wells, provided the test was long enough to develop the linear behaviour, and not long enough to be affected by boundaries.

Still in the line of dynamic connectivity metrics, *Bruderer-Weng et al.* [2004] quantified flow channeling in heterogeneous, exploring the effect of pore size correlation length in individual realizations. *Knudby and Carrera* [2005] proposed and evaluated the performance of nine dynamic connectivity indicators, amongst them three representative of flow connectivity. The authors concluded that all flow connectivity indicators succeeded in identifying the presence of high K features. *Trinchero et al.* [2008] presented an explicit mathematical framework that assessed the meaning of point-to-point transport connectivity in heterogeneous aquifers through the study of S_{est} combined with an indicator obtained from the analysis of tracer curves, ϕ_{est}. The authors found an analytical relationship between S_{est} and ϕ_{est}, and concluded that the processes governing transport connectivity were distinct from those involved in flow connectivity. *Frippiat et al.* [2009] investigated head and velocity variances as parameters that could provide valuable information about the occurrence of flow barriers and preferential pathways. Semi-analytical expressions for effective permeability, head variance and velocity variance were derived for saturated 2D anisotropic media and compared with results from numerical simulations of steady-state flow in random *K* fields, finding that

134 the solution fitted poorly in terms of head variances, but quite well for velocity
135 variances.

136 The most recent works regarding dynamic connectivity metrics include *Le Goc et al.*
137 [2010] who introduced two channelling indicators based on the Lagrangian distribution
138 of flow rates characterizing the extremes of the flow tube width distribution and the
139 flow rate variation along the flow paths. These indicators provide information on the
140 flow channel geometry and are applicable to both porous and fractured media. Finally,
141 *Bianchi et al.* [2011] investigated flow connectivity in a small portion of an extremely
142 heterogeneous aquifer after extracting 19 soil cores, yielding 1740 hydraulic
143 conductivity granulometric estimates and finally generating conditional realizations of
144 3-D K fields. The flow metrics obtained in the simulations were consistent with one of
145 the dynamic connectivity metrics proposed by *Knudby and Carrera* [2005].

146 In some studies static and dynamic connectivity metrics have been related. An example
147 is *Samouëlian et al.* [2007] who investigated the impact of topological aspects of
148 heterogeneous material properties on the effective unsaturated hydraulic conductivity
149 function, finding that the connectivity can best be represented by two topological
150 parameters (Euler-number and percolation theory). Also *Willmann et al.* [2008] studied
151 the relationship between breakthrough curves and dynamic indicators finding a
152 relationship between the slope of the late time breakthrough curves and two of the
153 dynamic metrics proposed by *Knudby and Carrera* [2005]. Most recently, *Henri et al.*
154 [2015] demonstrated that enhanced transport connectivity might have consequences on
155 human health risk assessment, largely controlling the location of high risk areas or hot
156 points in heterogeneous aquifers.

157 Connectivity patterns can also be included in the framework of multiple point
158 geostatistics (MPG). For example, *Renard et al.* [2011] and *Mariethoz and Kelly* [2011]
159 proposed algorithms to condition stochastic simulations of lithofacies to connectivity
160 information, by using a training image to build a set of replicates of conductivity fields
161 displaying connected paths that were consistent with the prior model.

162 The idea of connectivity related to the spatial patterns of conductivity is the basis of our
163 work. This same idea led *Fernàndez-Garcia et al.* [2010] to propose a methodology to
164 use the values obtained from tracer tests regarding travel times [following the

formulation of *Trinchero et al.*, 2008] to be used in transmissivity map delineation in a geostatistical framework. Here we follow a similar approach extended now to flow connectivity indicators. We thus propose a method to use the values of S_{est} that would be obtained from the interpretation of pumping tests using the Cooper-Jacob method combined with any existing value of local transmissivity, to map the best estimate of local T and the corresponding estimation uncertainty. The approach can be classified in the cokriging methods family and has as a significant point that the secondary variable is provided as a weighted integral of the (unknown) values of the primary variable. The method is then tested with a synthetic aquifer displaying statistical anisotropy of the local T values, where it is found that the inclusion of S_{est} values in the derivation allow getting a better representation of the presence of connected structures, as well as in the delineation of anisotropy.

2. Stochastic estimation of log-T fields using connectivity flow indicators

2.1 Background: Interpretation of pumping tests by the Cooper-Jacob method

Long-term pumping tests are common field hydraulic experiments to obtain estimates of hydraulic parameters. The traditional interpretation used by practitioners is the Cooper-Jacob (C-J) approach. It is relevant here to make a note of caution; the C-J approach has a range of validity that can be explored by using diagnostic plots [*Renard et al.*, 2008] before any interpretation is considered. The C-J method allows obtaining estimated values of transmisivity (T_{est}) and storage coefficient (S_{est}), but only in an apparent sense (that is, conditioned to the hypotheses underlain in the interpretation method used). In particular, the method is based on assuming homogeneous isotropic medium, so that all the effects of heterogeneity and anisotropy are directly transferred and embedded into the estimated apparent parameters. Different approaches mention this deficiency and have proposed alternatives to either obtain information about the parameters describing heterogeneity [*Copty et al.*, 2008; *Copty et al.*, 2011] or anisotropy [*Neuman et al.*, 1984] from the drawdowns recorded in a suite of observation points.

Meier et al. [1998] showed that even in heterogeneous porous and fractured media, the drawdown versus log time data recorded from long-term pumping tests were arranged

195 in a straight line for large times, therefore allowing the estimation of the slope (m) and
196 the intercept (with the X-axis, t_0) of this line. Knowing the pumping rate (Q) and the
197 distance between the pumping and the observation wells (r) two values can be derived

198 $$T_{est} = 0.183\frac{Q}{m}, \quad (1)$$

199 $$S_{est} = \frac{2.25T_{est}t_0}{r^2}. \quad (2)$$

200 It is well known that when this methodology is used in homogeneous aquifers, the
201 resulting parameters are precisely the transmissivity and the storage coefficient of the
202 aquifer (assuming no influence of boundary conditions).

203 In most aquifers hydraulic conductivity or transmissivity are highly variable in space,
204 while storage coefficient displays a lesser degree of variability as it is function of
205 porosity, compressibility of water and the mineral skeleton, all of them variables that
206 display low ranges of variability [see e.g. *Bachu and Underschulz*, 1992; *Neuzil*, 1994;
207 *Ptak and Teutsch*, 1994].

208 **2.2 Pumping tests in heterogeneous media**

209 The estimates from (1) and (2) are just two numbers that can be obtained regardless the
210 degree of variability of the real T and S fields. The obvious question is what is the
211 physical meaning of these estimated parameters when the medium is heterogeneous?
212 *Sanchez-Vila et al.* [1999] found analytically using a truncated perturbation expansion
213 (in log-T) of the flow equation in heterogeneous porous media that T_{est} obtained from
214 (1) is a good estimator of the effective transmissivity of the full field. The direct
215 consequence is that the tests are long enough, the estimates from different tests
216 performed in the same area would provide the same T_{est} value (so, performing more
217 than one test is uninformative in terms of estimates of transmissivity).

218 On the contrary, S_{est} from (2) is an observation point dependent parameter that weight
219 averages the local T values lying in an area that includes the pumping and the
220 observation wells. The actual integral is given as [*Sanchez-Vila et al.*, 1999]

$$S_{est}(r,\theta) = S\,\exp\left(-\int_{\Re^2} U\left(r,\theta,\rho,\phi\right) Y'\left(\rho,\phi\right)\rho\, d\rho\, d\phi\right), \tag{3}$$

where $Y'(\boldsymbol{x}) = \ln\left(T(\boldsymbol{x})/T_{eff}\right)$, and U is a weighting function (kernel) given by

$$U\left(r,\theta,\rho,\phi\right) = -\frac{\rho - r\,\left(\cos\theta - \phi\right)}{\rho\left(\rho^2 + r^2 - 2\rho r\,\left(\cos\theta - \phi\right)\right)}\,, \tag{4}$$

where (ρ,ϕ) are the polar coordinates centered at the observation point, (r,θ) are the polar coordinates centered at the pumping well.

Thus, S_{est} values provide more information of the underlying heterogeneous structure of the local T value than T_{est}, indicating the potential of the former variable to be incorporated into a methodology for mapping local transmissivities (while T_{est} are mostly useless for that purpose). Moreover, S_{est} directly incorporates the response time of a given location to pumping (as it includes the intercept time, which is an indirect measure of response time), which can be directly transferred to a connectivity index as suggested by *Fernàndez-Garcia et al.* [2010], who defined explicitly the flow connectivity indicator (w') as

$$\omega' = \ln\left(\frac{S_{est}}{S}\right), \tag{5}$$

where S is the actual storage coefficient (assumed constant for simplicity, but an effective value could also be used if heterogeneity in local S values was considered). From this definition negative values of w' represent good flow connectivity between pumping and observation well, and positive values otherwise.

2.3 The flow connectivity estimator

Combining (3) and (5), the flow connectivity indicator can be written as a weighted average of the deviations of the log-T values with respect to the effective T value, where the weighting function is a Fréchet Kernel given already in (4), as

$$\omega'\left(r\,,\theta\right) = -\int_{\Re^2} U\left(r,\theta,\rho,\phi\right) Y'\left(\rho,\phi\right)\rho\, d\rho\, d\phi \tag{6}$$

where the local polar coordinates considers the pumping well as the origin of coordinates. The shape of function U deserves some comments (see Figure 1); it displays two singularities (infinite value) at the location of the pumping well and observation point, is equal to zero along the circumference drawn by considering the diameter as that formed by these same two points, it is positive in all values located inside the circle, and negative outside, with values tending to zero as the distance to the circumference increases. Essentially this Kernel function expresses that the pumping location is well connected to an observation point when high transmissivity values are displayed in the area closer to the two points and (relatively) small transmissivity values concentrate outside of the influence area (the circumference specified).

2.4 Estimation by means of a cokriging approach

At any location where local T has not been sampled, we need to estimate the corresponding value to draw a map of the best estimates for local T values. We use here the geostatistical method known as cokriging. We start by defining the linear estimator of $Y(\boldsymbol{x}_0)$ as

$$Y_{CK}(\boldsymbol{x}_0) = \sum_{i=1}^{n_Y} l_i^Y Y_i + \sum_{j=1}^{n_w} l_j^w w'_j \qquad (7)$$

where $Y_{CK}(\mathbf{x}_0)$is the estimator of log Transmissivity in a certain point $\boldsymbol{x}_0$, $l_i^Y(\mathbf{x}_0)$ and $l_i^w(\mathbf{x}_0)$, both location and data dependent, are the weights applied to values of log-Transmissivity (Y_i) and flow connectivity (w'), which by convention is defined as $w'_i = w'(\boldsymbol{x}_i, \boldsymbol{x}_p)$, where $\boldsymbol{x}_i$ and $\boldsymbol{x}_p$ are the observation point and the pumping well locations, respectively. Here it is important to state that w' is symmetric with respect to the two points. Still in (7), n_Y, n_w represent the data of each type used in the estimation process.

The relative weight of each of the variables is based on the spatial distribution of the observation points. We describe $Y(\boldsymbol{x}) = \ln T(\boldsymbol{x})$ as a correlated random function, fully defined by its expected value m_x and a two-point covariance function C^{YY}. From 86),

the attribute w' is linearly dependent on Y and can be described as a correlated random function with zero mean.

As in all cokriging methods, the weighting coefficients are obtained by applying the conditions of unbiasedness and minimum variance of the estimator error. The most relevant details of the mathematical derivation are presented in the Appendix. The main results are presented here.

The unbisedness condition, implying that $\langle Y_{CK} \rangle = m_Y$, leads to

$$\sum_{i=1}^{n_Y} l_i^Y = 1. \tag{8}$$

The second condition, the minimization of the variance of the estimator error, $s_{CK}^2 = E\{(Y_{CK} - Y)^2\}$ implies developing the full expression for s_{CK}^2 (see equation A.4) and then minimizing a Lagrangian function that includes the unbiasedness constraint (equation A.3). This results in a linear system of $k + l + 1$ equations with $k + l + 1$ unknowns that we reproduce here

$$\begin{aligned}
&\sum_{i=1}^{n_Y} l_i^Y C_{ik}^{YY} + \sum_{j=1}^{n_w} l_j^w C_{jk}^{Yw} - m = C_{k0}^{YY}, \qquad k = 1,...,n_Y \\
&\sum_{i=1}^{n_Y} l_i^Y C_{il}^{Yw} + \sum_{j=1}^{n_w} l_j^w C_{jl}^{ww} = C_{l0}^{Yw}, \qquad l = 1,...,n_w \\
&\sum_{i=1}^{n_Y} l_i^Y = 1
\end{aligned} \tag{9}$$

The method then implies that at each point $\mathbf{x}_0$ in a predefined mesh we assign an estimated value of local T obtained by performing the following steps:

1) Solving equation (9) for $l_i^Y (i = 1,...,n_Y)$, $l_j^w (j = 1,...,n_w)$, m,
2) obtain $Y_{CK}(\mathbf{x}_0)$ from equation (7),
3) compute s_{CK}^2 from equation (A.6).

A critical point in step (1) is the evaluation of the covariance and cross-covariance functions, that can all be written in terms of integrals of be obtained as C^{YY}:

$$C^{Yw}(\boldsymbol{x}_i,\boldsymbol{x}_j) = -\int_{\hat{A}^2} U(\boldsymbol{x}_j,\boldsymbol{x}) C^{YY}(\boldsymbol{x}_i,\boldsymbol{x}) d\boldsymbol{x}, \quad (9)$$

$$C^{ww}(\boldsymbol{x}_i,\boldsymbol{x}_j) = \int_{\hat{A}^2}\int_{\hat{A}^2} U(\boldsymbol{x}_i,\boldsymbol{x}') U(\boldsymbol{x}_j,\boldsymbol{x}'') C^{YY}(\boldsymbol{x}',\boldsymbol{x}'') d\boldsymbol{x}' d\boldsymbol{x}'' . \quad (10)$$

2.5 Mathematical code implementation

The set of equations composed by (7), (9)-(11) and (A.6) were implemented in ad-hoc code programmed in Matlab [*MathWorks*, 2014]. The implementation of the variance-crossvariance matrices in equations (9)-(10) are calculated numerically at each cell, based on the numerical integration of the covariance of the log-T values times a Kernel function. If there is an observation point containing both Y and w' data, the order of assembly of the cross-covariance matrix is done sequentially. The integrals in (9)-(10) are solved using different types of programming loops; at those points where the U function presents singularities (pumping well and observation point), the sums are performed with the values corresponding to the centre of the cells, with the singular points located at the edges of the cells, avoiding such singularities.

Once the covariance functions are estimated, the solution of (9) is straight forward, being a system of linear equations.

3. Development of a synthetic model and hydraulic parameters obtaining

3.1 Construction and modeling of the synthetic aquifer

The flow model constructed in the finite differences code Modflow incorporated in model ModelMuse [*USGS*, 2015] considers a square domain of size 2600 units. This domain is discretized into 406 x 406 square cells of variable size, being most refined inside the inner region where the pumping tests are simulated. The outer region is used to prevent boundary effects. The cell size in the inner domain is of one unit, then increases outside this region following a geometric progression with a factor 1.2. The inner region consist of 300 x 300 cells. We further defined a simulation domain located within the inner region, that corresponds to the area where both the pumping and observation wells are located. The natural log of the transmissivity field in the inner and simulation regions is modeled as a Gaussian anisotropic structure with a sill of 1, a

mean of 0, and ranges of 15 and 30 units in the X and Y direction. We consider one realization of such field, performed with SGeMS [*Remy and Boucher*, 2009], presented in Figure 2. The storage coefficient is constant and equal to $S=10^{-2}$ for the entire domain. The transmissivity field outside the inner region is assumed constant and equal to $Y = \ln T = 0$. The head level at the boundaries is prescribed at h=0. Figure 3 shows a sketch of the numerical setup, where the heterogeneous conductivity inner domain and homogeneous outer domain are represented. Distances are given in terms of spatial range correlations.

Three different pumping tests are performed in order to find flow connectivity indicator values (w') between pumping and observation wells. Each test involves a different pumping well, but the six observation points are common for all tests. This set up produces a total of 18 w' values. A period of 11000 time units is simulated, where each of the abstraction wells separately pump for a period of 3100 units, sufficient to obtain a late straight line in the Cooper-Jacob interpretation, and so that boundary effects do not have any effect. As the model is two-dimensional, we implicitly assume fully penetrating wells. The flow rate in each test is 50 [L^3 T^{-1}], a value selected from preliminary runs. Two well distributions are considered, a first one consisting in a regular well distribution, and a second one with a deliberated well distribution placing wells in those zones where the values of Y are either very high or very low. The entire mesh, the simulating domain K field and the two well distribution configurations are shown in Figure 4.

3.2 Pumping tests modelling results. Estimation of connectivities

Once pumping tests were performed, T_{est} and S_{est} are computed from (1) and (2) respectively. In Table 1 all estimated values, as well as sampled T values, are compiled for the two well distribution arrangements. The w' values, obtained from (5), are also reported; these values were obtained using $S = 1\text{x}10^{-2}$ (notice that the geometric mean of all reported S_{est} values is exactly equal to $1\text{x}10^{-2}$, confirming the theoretical results of *Sanchez-Vila et al.* [1999]).

Table 1. Values of flow connectivity obtained for the case of regular and deliberated distributed wells.

Pumping Well	Observation well	Regular distributed wells				Deliberated distributed wells			
		T_{est}	T_{real}	S_{est}	w'	T_{est}	T_{real}	S_{est}	w'
A	Obs.1	0.98	0.29	1.14E-2	**0.13**	0.98	1.49	9.67E-3	**-0.03**
	Obs.2	1.01	0.15	1.40E-2	**0.33**	0.99	0.07	1.17E-2	**0.16**
	Obs.3	0.98	3.91	1.16E-2	**0.15**	0.99	2.32	1.31E-2	**0.27**
	Obs.4	1.01	1.47	1.11E-2	**0.11**	0.99	5.70	9.61E-3	**-0.04**
	Obs.5	0.99	1.53	7.77E-3	**-0.25**	1.02	0.11	1.23E-2	**0.21**
	Obs.6	1.01	3.71	8.73E-3	**-0.14**	1.03	0.42	1.11E-2	**0.11**
B	Obs.1	1.01	0.29	6.81E-3	**-0.38**	1.03	1.49	7.12E-3	**-0.34**
	Obs.2	1.03	0.15	1.78E-2	**0.58**	1.02	0.07	1.00E-2	**0.002**
	Obs.3	1.01	3.91	1.22E-2	**0.20**	1.02	2.32	9.82E-3	**-0.02**
	Obs.4	1.02	1.47	1.77E-2	**0.57**	2.03	5.70	4.89E-3	**-0.72**
	Obs.5	1.02	1.53	8.83E-3	**-0.12**	1.04	0.11	1.25E-2	**0.22**
	Obs.6	1.01	3.71	1.31E-2	**0.27**	1.03	0.42	1.81E-2	**0.59**
C	Obs.1	1.04	0.29	1.01E-2	**0.01**	1.06	1.49	9.76E-3	**-0.02**
	Obs.2	1.03	0.15	8.92E-3	**-0.11**	1.05	0.07	8.34E-3	**-0.18**
	Obs.3	1.04	3.91	1.08E-2	**0.08**	1.04	2.32	1.31E-2	**0.27**
	Obs.4	1.01	1.47	5.23E-3	**-0.64**	1.04	5.70	1.18E-2	**0.17**
	Obs.5	1.04	1.53	9.48E-3	**-0.05**	1.04	0.11	1.10E-2	**0.10**
	Obs.6	1.03	3.71	1.78E-2	**0.58**	1.02	0.42	1.07E-2	**0.07**

As Table 1 reflects, the values of estimate transmissivity T_{est} are quite homogeneous, confirming the results of *Meier et al.* [1998] and *Sanchez-Vila et al.* [1999]. Actually the reported T_{est} values are very close to 1 [L^2/T] (i.e., $\langle Y \rangle = 0$) while the real T values (T_{real}) are quite heterogeneous. Again, the repetition of pumping tests to obtain T_{est} values would be uninformative. On the other hand, the values of S_{est} vary up to half order of magnitude in selected points; i.e., all information in heterogeneity is then transferred to the S_{est} values. The reported w' values are displayed graphically in Figure 5, with emphasis in the sign (negative values in green indicating good connectivity, and positive ones in red are indicative of bad connectivity) and in the magnitude (represented by the thickness of the lines).

As demonstrated in both Figure 5 and Table 1, there are several tendencies in the reported w' values, as compared to the corresponding local Y values at both pumping well and observation point. First, as expected, there are some negative w' values in those pair of wells located in high Y zones. This tendency is observed in the regular distributed wells case, specifically in Well A-Observation 5, Well B-Observation 1 and Well C-Observation 4, this last showing a greatly exaggerated connectivity value caused by the existence of a continuous high Y zone directly connecting these two points. In the case of deliberated distributed wells, these negative w' relationships are observed in Well A-Observation 1 and Observation 4, and Well B-Observation 1 and Observation 4.

On the contrary, there is some bad connected well pairs located in zones of low Y values (whether the two points or only one of them). These can be seen in the w' values between Well A-Observation 2 and Well B-Observation 2 and Observation 4 (regular distributed wells) and in Well A-Observation 2 and Observation 5, Well B-Observation 5 and Observation 6 and Well C-Observation 3 and Observation 5 (deliberated distributed wells). An important factor that needs to be considered is that the distance between the pumping and the observation wells (r) can sensibly influence the results of S_{est} and therefore w' in the calculation of S_{est} (3) by the C-J interpretation. For example, it would result in more negative w' values than expected (and therefore read as having a high connectivity) at very large distances, and more positive w' values than expected at short distances. An example of anomalous positive w' can be observed in the pair Well A-Observation 3, Well B-Observation 6 and Well C-Observation 6 for

380 regular distributed wells and in Well A-Observation 3 for deliberated distributed wells.
381 Anomalous negative w' values can be seen in Well C-Observation 2 for regular wells
382 distribution and Well C-Observation 2 for deliberated wells distribution.

383 **3.3 Map reconstruction of the local T values**

384 From the values of w' presented in Table 1, and taking into account the point Y values
385 assumed known without errors in all pumping and observation wells (taken from the
386 reference Y map), we present here the result of the cokriging method to reconstruct the
387 original log transmissivity field. One of the immediate effects of using a cokriging
388 method is that the maps obtained display smoothed shapes, contrary to the maps
389 obtained by means of methods based on conditional simulations.

390 **Case 1: Regular distributed wells scenario**

391 Figure 6 displays several reconstructed point T values depending on the amount and
392 type of data used in the estimation process. First, for case (b), where a simple kriging
393 using point Y data and not considering flow connectivity data is performed, the
394 resulting map shows the anisotropy, reflecting the continuity in the Y structures in the
395 Y-direction originated by the structure of the theoretical variogram (with an anisotropy
396 ratio of 2). Map (c) is obtained after incorporation of the w' values; it is perceived the
397 difficulty to analyse each of the relationships of the connectivity between all points
398 individually because there is much redundant information; nevertheless there are some
399 connectivity relationships that are clearly observed, modifying the Y estimates as a
400 function of the sign of the w' values. This is observed, for example, in the relationship
401 between Well A and Observation 1, where the high connectivity (w'= -0.38) affects the
402 estimates as compared to map (b). The opposite happens in the relationships between
403 Well B and Observations 3, 4 and 6 and Well C and Observation 6, where the values of
404 interpolated Y decrease respect to the field of map (b) due to low connectivity values
405 between these wells (w'=0.20, 0.57, 0.27 and 0.58 respectively). Some of the
406 continuous low T structures reflected in the initial Y field (a) are visible in map (c),
407 while not represented in map (b).

408 In map (d), the point Y values are omitted in the interpolation (l_i^Y=0), thus only the w'
409 values are used. It can be observed that results show negative connectivity w' values,

and hence higher values of interpolated Y field especially, for the relationships between Well A-Observation 5 and 6, the latter not very clearly visible due to the large amount of crossed information existing in this particular zone and for Well B-Observation 1 and Well C-Observation 4. On the other hand, positive connectivity values are reflected in Well A-Observation 3, although these values are influenced by the values of high connectivity between Well A and observation 5, Well B and observations 2 and 4, and finally Well C and observation 6 (see Table 1). Another significant result is the presence of reverse shadow areas that are caused by the shape of the function U used to calculate covariance matrices, displaying negative values of U behind the pumping and observation wells. These reverse shadow zones can be observed on the right side of Observation well 2, originated by the low w' values between this point and pumping wells A and B. Another reverse shadow zone is observed south of the Observation 6, where this high interpolated Y zone is caused by the positive connectivity w' values between this point and pumping wells B and C. Finally, another high Y interpolated shadow zone is located in the left slot of Well A and Observations 3 and 5 caused by the positive connectivity w' values of all pumping wells with observation 3. Otherwise, a low Y reverse shadow area appears on top of Observation 1, caused by the negative connectivity w' value between this observation and Well B.

Case 2: Deliberated distributed wells scenario

In this case, both pumping and observation wells are distributed strategically to better reflect the extreme values of the actual Y field, and be able to observe how this distribution, together with the integrated values of w' affects the results of the final interpolated maps. In Figure 7 all interpolated maps considering this deliberated well distribution are reflected.

This setup implies that in the maps from Figure (7) there is a better reproduction of the extremes of the pdf of local T as compared to those in Figure 6, but also the continuity of structures (whether of high or low conductivity). This is quite evident in map (b) when the two figures are directly compared. In map (c) the introduction of w' values in the interpolation are also quite efficient in showing the continuity of structures as compared to map (b). First, the introduction of w' data is visible in the vicinity of Well B and Observation 3 and Well C with observations 5 and 6, lowering Y interpolated

441 values in the former, and rising them in the latter, as compared to map (b). Moreover,
442 new stripes of low Y values are displayed (again as compared to map (b)) due to the
443 overall presence of positive w' values. Nevertheless high Y interpolated values stripes
444 also appear in the area between Well C and Observation 5 and also on the right side of
445 well C. High Y interpolated stripes would appear as a consequence of reverse shadow
446 zones caused by the positive w' values between Wells A and B and Observation 5 in
447 the former case, and for the positive connectivity values between Well B and
448 Observation 6 in the latter one.

449 As the relative weights of sampled Y (l_i^Y) are removed, it is observed how the values of
450 negative w' are represented with zones of high Y. This happens, for example, in the
451 area located between Well B and Observation 4, where the Y interpolated values are
452 high, although a shadow zone of low Y is originated behind Observation 4 (caused by
453 this negative w' value). On the other hand, positive connectivity values are observed,
454 for example, in the zone located between Well B and Observation 6, and the consequent
455 presence of a shadow zone of high Y east of Observation 6.

456 **4. Validation and relevance of the work**

457 **4.1 Validation of results through new simulations**

458 In order to analyse the reliability regarding the reproduction of the different flow
459 connectivity patterns of the initial synthetic aquifer, all the reconstructed T fields are
460 tested to see their capability of reproducing the results of additional pumping tests.
461 Figure 8 shows the position of pumping and observation wells in a new configuration of
462 tests, comprising four pumping wells and eight observation wells.

463 The validation method proceeds as follows. Pumping tests are simulated in the original
464 T field. Cooper-Jacob's method is used to obtain S_{est} and subsequently calculate w'
465 values corresponding to the 32 combinations of pumping and observation wells. The
466 same procedure is repeated for all the estimated T fields presented in figures 6 and 7 (a
467 total of 6 fields). Finally, the resulting w' values are compared in a regression plot
468 (Figure 9). Table 2 shows the information used in each estimated Y field.

469 **Table 2.** Information used in each Y interpolated field.

Scenario	Information used as observed values	Description
a	9 T_{real} values	Simple kriging using Y values
b	9 T_{real} values + 18 w' values	Cokriging using Y and w' values
c	18 w' values	Cokriging using w' values. Transmissivity weights (l_i^Y) are set to 0.

As referring to the w' results obtained taking into account regular distributed wells and comparing with w' results obtained with the initial Y field, it is observed that the values of regression line of (a) r^2=0.20 indicate virtually no correlation, in general overestimating the degree of connectivity between almost all of the points considered with respect to the values obtained from the original T field. Case b shows a significant improvement with respect the case a, improving the values of r^2 and m (slope of the regression line between connectivity indicator calculated on reconstructed Y fields and the reference Y field). On the other hand, if only w' values were used in the mapping process, the reconstruction of the new pumping tests is quite bad (r^2=0.18 and m =0.27). Therefore, considering these three interpolated maps (regular well configurations), the option that best represent the initial field in terms of connectivity, is that in which in the interpolation considers both Y and w' values (b).

In the deliberated distributed wells case, the general behaviour is the same as that discussed in the regular distributed wells, being the interpolated map considering the values of Y and w' (b) that best represent the results obtained in the initial field (r^2 =0.75; m =0.71), regarding the flow connectivity patterns obtained. However, there is a substantial difference in results of r^2 and m obtained in this second distribution, being these much better for all cases respect to the regular distribution.

4.2 Relevance of the work

490 The method proposed provides interpolated T values based on either local Y or w'
491 values (or both). Actually, any map obtained from a method of the kriging family
492 (cokriging here) has no chance of properly reproducing the T field and provides always
493 a smoothed version of the real map.

494 Here we explore the main difference in the maps obtained by using only local Y values
495 or incorporating also some w' values. The difference is quite mild in terms of
496 comparing the maps in Figures 6 and 7; the improvement can only be assessed in terms
497 of performance of the reconstructed fields. For this purpose we performed transport
498 simulations. We considered the introduction of a solute mass through the southern
499 boundary of the original plus the two interpolated fields. The method consisted on
500 applying a head difference between the southern and northern boundaries, solving the
501 flow field under these flow conditions (eastern and western boundary are specified as
502 no-flow, and no pumping was included). Then 300 particles were injected at the inlet
503 (uniformly distributed) and collected at the northern one. Figure 10 shows the
504 cumulative mass as a function of time for all cases.

505 From Figure 10 we see first that interpolated maps cannot reproduce the cumulative
506 mass shape of the real T field. All interpolated maps are smoothed versions and
507 therefore do not properly reproduce early and late time mass arrivals. The introduction
508 of the w' data results in a few more channels of high T developing in the system (notice
509 the enhancement in early arrivals), so that it results in a more conservative approach to
510 solute transport to a comply surface (as compared to ignoring those values). Comparing
511 the transport simulations obtained using the interpolated fields with those associated
512 with the real one, we can see that these fast channels actually exist and are crucial for
513 risk assessment.

514 Finally, we also want to insist in the fact that w' values are quite robust, as they come
515 from a graphical fitting method. On the contrary, there is much more error in the
516 estimation of the local T values at some predefined scale. We contend that the inclusion
517 of w' should then be considered a must if they are available in a real case.

518

519 **5. Conclusions**

520 We analyse the applicability of the flow connectivity indicator parameter w', calculated
521 from the value of S_{est} obtained in a pumping test using Cooper-Jacob's interpretation
522 method. The rationale behind is the idea that it provides integrated information about
523 the spatial distribution of local T values displayed in the area surrounding the pumping
524 well and the observation point. Based on this idea it is possible to devise a method that
525 uses the values of w' obtained in a number of hydraulic test performed in a given area,
526 together with any existing point T values to map the best estimate of the T map in a
527 cokriging approach. The method is tested numerically by reconstructing maps
528 depending on different density of data points of w' and T and then testing the capability
529 of reproducing new pumping tests. Our work leads to the following conclusions:

530 1. w' is a reliable indicator of flow connectivity between a pumping and an
531 observation well. Contrarily, local T values cannot be properly assessed as they heavily
532 rely on the interpretation method and, more, it is difficult to assign the estimated values
533 to a precise support volume.
534 2. Flow connectivity values (w') found in an anisotropic heterogeneous medium
535 can display some unexpected values due to the presence of low or high transmissivity
536 structures that act either as flow barriers, or as preferential pathways. However, in some
537 cases it can be overestimated whenever the distance between the pumping and
538 observation well is large (and underestimated if it is small) due to the effect of the
539 kernel function involved in the definition
540 3. The incorporation of the available w' values result in a best reproduction of the
541 estimated map of local T values through a cokriging method, as compared to the one
542 obtained by using only local T data in a kriging approach. In particular, the cokriging
543 approach provides maps that display more extreme values and that are better capable of
544 reproducing the shape of the drawdown curves if new pumping tests were considered.
545 4. The method provides the best results when pumping and observation wells are
546 located in extreme (high or low) areas of local T, implying the need for a proper
547 assessment of the potential location of such values if possible.
548 5. The number of local T values used in the interpolation is also very relevant,
549 indicating the need to combine long-term pumping tests to obtain mainly w' values,
550 with any hydraulic test conducive to the evaluation of T values at the local scale (e.g.
551 Slug test) with the purpose of obtaining the lowest degree of homogeneity in the T

552 values, contrary that what occurs in the Cooper-Jacob interpretation. It must be clarified
553 that this type of point hydraulic tests might involve a large degree of error in the
554 evaluation of local T and S values.
555 6. As a consequence of the introduction of the function U when calculating the
556 covariance matrices, the final Y interpolated maps show shadow zones behind the
557 observation and pumping wells, creating a zone of low transmissivity if the connectivity
558 between the points is negative (high transmissivity values) and vice versa. The best way
559 to minimize the occurrence of these shadow zones is to incorporate as much as crossed
560 information as possible into the interpolation. Another measure to consider, is to omit
561 those interpolated information that falls outside the perimeter created when connecting
562 the points located at the extremes.

563

564 **Appendix: Derivation of the cokriging equations**

565 The starting point is equation (7), which is reproduced here

566 $$Y_{CK}(\boldsymbol{x}_0) = \sum_{i=1}^{n_Y} l_i^Y Y_i + \sum_{j=1}^{n_w} l_j^w w'_j \qquad \text{(A.1)}$$

567 The unbiasedness condition is obtained by taking expected value (operator $\langle\ \rangle$) at both
568 sides of (A.1). Since $\langle w' \rangle = 0$ and $\langle Y \rangle = m_Y$, then we obtain

569 $$\langle Y_{CK} \rangle = \sum_{i=1}^{n_Y} l_i^Y m_Y \qquad \text{(A.2)}$$

570 Unbiasedness implies that $\langle Y_{CK} \rangle = m_Y$, which is equivalent to $\sum_{i=1}^{n_Y} l_i^Y = 1$, corresponding
571 to equation (8).

572 The second condition of the cokriging method is the minimization of the variance of the
573 estimator error, $s_{CK}^2 = E\left\{(Y_{CK} - Y)^2\right\}$ under the unbiasedness constraint. This requires
574 the minimization of the (Lagrangian) objective function L, involving one Lagrangian
575 parameter m

576 $$L\left(\lambda_i^Y, \lambda_i^w, m\right) = \frac{1}{2} E\left[\left(Y_{CK} - Y\right)^2\right] - m\left(\sum_{i=1}^{n_Y} \lambda_i^Y - 1\right) \quad \text{(A.3)}$$

577 We start by developing an expression for s_{CK}^2

578 $$\begin{aligned} s_{CK}^2 = E\left[\left(Y_{CK} - Y\right)^2\right] = & \sum_{i=1}^{n_Y}\sum_{j=1}^{n_Y} \lambda_i^Y \lambda_j^Y C_{ij}^{YY} + \sum_{i=1}^{n_w}\sum_{j=1}^{n_w} \lambda_i^w \lambda_j^w C_{ij}^{ww} \\ & + 2\sum_{i=1}^{n_Y}\sum_{j=1}^{n_w} \lambda_i^Y \lambda_j^w C_{ij}^{Yw} - 2\sum_{i=1}^{n_Y} \lambda_i^Y C_{i0}^{YY} - 2\sum_{j=1}^{n_w} \lambda_j^w C_{j0}^{Yw} + E\left[Y^2\right] \end{aligned} \quad \text{(A.4)}$$

579 The optimization process consists of substituting (A.4) in (A.3) and then solving the

580 following linear system of equations $\frac{\partial L}{\partial \lambda_i^Y} = 0, \frac{\partial L}{\partial \lambda_i^w} = 0, \frac{\partial L}{\partial m} = 0$, resulting in a linear

581 system of $k + l + 1$ equations with $k + l + 1$ unknowns

582 $$\begin{aligned} & \sum_{i=1}^{n_Y} \lambda_i^Y C_{ik}^{YY} + \sum_{j=1}^{n_w} \lambda_j^w C_{jk}^{Yw} - m = C_{k0}^{YY}, \qquad k = 1,\ldots,n_Y \\ & \sum_{i=1}^{n_Y} \lambda_i^Y C_{il}^{Yw} + \sum_{j=1}^{n_w} \lambda_j^w C_{jl}^{ww} = C_{l0}^{Yw}, \qquad l = 1,\ldots,n_w \\ & \sum_{i=1}^{n_Y} \lambda_i^Y = 1 \end{aligned} \quad \text{(A.5)}$$

583 The cokriging system is complemented by a closed-form evaluation of the variance of

584 the estimation error, becoming

585 $$s_{CK}^2 = E\left[\left(Y_{CK} - Y\right)^2\right] = E\left[Y^2\right] - \sum_{i=1}^{n_Y} \lambda_i^Y C_{i0}^{YY} - \sum_{j=1}^{n_w} \lambda_j^w C_{j0}^{Yw} + m \quad \text{(A.6)}$$

586

587 **Acknowledgements**

588 Partial provided support was provided by ENRESA (Empresa Nacional de Residuos,
589 S.A.). XS acknowledges support from the ICREA Academia Program. All data used
590 was synthetically generated and is available upon request to the corresponding author.

591 **References**

592 Attinger, S. (2003), Generalized coarse graining procedures for flow in porous media,
593 Computational Geosciences, 7(4), 253-273.
594 Bachu, S., and J. R. Underschulz (1992), Regional scale porosity and permeability variations,
595 Peace River Arch area, Alberta, Canada, AAPG Bull., 76(4), 547-562.
596 Bianchi, M., C. Zheng, C. Wilson, G. R. Tick, G. Liu, and S. M. Gorelick (2011), Spatial
597 connectivity in a highly heterogeneous aquifer: From cores to preferential flow paths, Water
598 Resources Research, 47(5), W05524.
599 Bour, O., and P. Davy (1997), Connectivity of random fault networks following a power law
600 fault length distribution, Water Resources Research, 33(7), 1567-1583.
601 Bruderer-Weng, C., P. Cowie, Y. Bernabé, and I. Main (2004), Relating flow channelling to
602 tracer dispersion in heterogeneous networks, Advances in Water Resources, 27(8), 843-855.
603 Cooper, H.H. Jr., and C.E. Jacob (1946), A generalized graphical method for evaluating
604 formation constants and summarizing well-field history, Transactions American Geophysical
605 Union, 27 (4), 526–534.
606 Copty, N. K., P. Trinchero, and X. Sanchez-Vila (2011), Inferring spatial distribution of the
607 radially integrated transmissivity from pumping tests in heterogeneous confined aquifers,
608 Water Resources Research, 47, Art No W05526.
609 Copty, N. K., P. Trinchero, X. Sanchez-Vila, M. S. Sarioglu, and A. N. C. W. Findikakis
610 (2008), Influence of heterogeneity on the interpretation of pumping test data in leaky
611 aquifers, Water Resources Research, 44(11).
612 De Marsily, G., F. Delay, J. Gonçalvès, P. Renard, V. Teles, and S. Violette (2005), Dealing
613 with spatial heterogeneity. Hydrogeology Journal, 13 (8), 161-183.
614 Deutsch, C. V. (1998), FORTRAN programs for calculating connectivity of three-dimensional
615 numerical models and for ranking multiple realizations, Computers & Geosciences, 24(1),
616 69-76.
617 Fernàndez-Garcia, D., P. Trinchero, and X. Sanchez-Vila (2010), Conditional stochastic
618 mapping of transport connectivity, Water Resources Research, 46(10), W10515.
619 Fogg, G. (1986), Groundwater flow and sand body interconnectedness in a thick, multiple
620 aquifer system., Water Resources Research, 22(5), 679-694.
621 Frippiat, C. C., T. H. Illangasekare, and G. A. Zyvoloski (2009), Anisotropic effective medium
622 solutions of head and velocity variance to quantify flow connectivity, Advances in Water
623 Resources, 32(2), 239-249.
624 Guimerà, J., and J. Carrera (1997), On the interdependence on transport and hydraulic
625 parameters in low permeability fractured media. Hard Rock Hydrosystems, IAHS Publ. no.
626 241.
627 Guimerà, J., and J. Carrera (2000), A comparison of hydraulic and transport parameters
628 measured in low-permeability fractured media, Journal of Contaminant Hydrology, 41(3–4),
629 261-281.
630 Henri, C. V., D. Fernàndez-Garcia, and F. P. J. de Barros (2015), Probabilistic human health
631 risk assessment of degradation-related chemical mixtures in heterogeneous aquifers: Risk
632 statistics, hot spots, and preferential channels. Water Resources Research, 51(6), 4086-4108.
633 Ji, S.-H., Y.-J. Park, and K.-K. Lee (2011), Influence of Fracture Connectivity and
634 Characterization Level on the Uncertainty of the Equivalent Permeability in Statically
635 Conceptualized Fracture Networks. Transport Porous Media, 87 (2), 385.
636 Knudby, C., and J. Carrera (2005), On the relationship between indicators of geostatistical, flow
637 and transport connectivity, Advances in Water Resources, 28(4), 405-421.
638 Knudby, C., J. Carrera, J. D. Bumgardner, and G. E. Fogg (2006), Binary upscaling—the role of
639 connectivity and a new formula, Advances in Water Resources, 29(4), 590-604.
640 Le Goc, R., J. R. de Dreuzy, and P. Davy (2010), Statistical characteristics of flow as indicators
641 of channeling in heterogeneous porous and fractured media, Advances in Water Resources,
642 33(3), 257-269.
643 Mariethoz, G., and B. F. J. Kelly (2011), Modeling complex geological structures with
644 elementary training images and transform-invariant distances, Water Resources Research,
645 47(7), W07527.
646 MathWorks (2014), MATLAB, edited, Natick, Massachusetts 01760 USA.

Meier, P. M., J. Carrera, and X. Sanchez-Vila (1998), An evaluation of Jacob's Method for the interpretation of pumping tests in heterogeneous formations, Water Resources Research, 34(5), 1011-1025.
Neuman, S. P. (2008), Multiscale relationships between fracture length, aperture, density and permeability, Geophysical Research Letters, 35(L22402), 6.
Neuman , S. P., G. R. Walter, H. W. Bentley, J. J. Ward, and D. Gonzalez (1984), Determination ofHorizontal Aquifer Anisotropy with Three Wells, Ground Water, 22(1), 6.
Neuweiler, I., A. Papafotiou, H. Class, and R. Helmig (2011), Estimation of effective parameters for a two-phase flow problem in non-Gaussian heterogeneous porous media, Journal of Contaminant Hydrology, 120–121(0), 141-156.
Neuzil, C. E. (1994), How permeable are clays and shales?, Water Resources Research, 30(2), 145-150.
Odling, N. E. (1997), Scaling and connectivity of joint systems in sandstones from western Norway, Journal of Structural Geology, 19(10), 1257-1271.
Pardo-Igúzquiza, E., and P. A. Dowd (2003), CONNEC3D: a computer program for connectivity analysis of 3D random set models, Computers & Geosciences, 29(6), 775-785.
Poeter, E., and P. Townsend (1994), Assessment of critical flow path for improved remediation management., Ground Water, 32(3), 439-447.
Ptak, T., and G. Teutsch (1994), A comparision of investigation methods for the prediction of flow and transport in highly heterogeneous formations, Transport and reactive processes in aquifers: Rotterdam, Balkema, 157-164.
Remy, N., A. Boucher and J.Wu (2009), Applied geostatistics with SGeMS, Cambridge University Press Publ.
Renard, P., and D. Allard (2013), Connectivity metrics for subsurface flow and transport, Advances in Water Resources, 51(0), 168-196.
Renard, P., D. Glenz, and M. Mejías (2008), Understanding diagnostic plots for well-test interpretation, Hydrogeology Journal, 17, 11.
Renard, P., J. Straubhaar, J. Caers, and G. Mariethoz (2011), Conditioning Facies Simulations with Connectivity Data, Mathemaical Geosciences, 43(8), 897-903.
Samouëlian, A., H. J. Vogel, and O. Ippisch (2007), Upscaling hydraulic conductivity based on the topology of the sub-scale structure, Advances in Water Resources, 30(5), 1179-1189.
Schad, H., and G. Teutsch (1994), Effects of the investigation scale on pumping test results in heterogeneous porous aquifers, Journal of Hydrology, 159(1–4), 61-77.
Schlüter, S., and H.-J. Vogel (2011), On the reconstruction of structural and functional properties in random heterogeneous media, Advances in Water Resources, 34(2), 314-325.
Schulze-Makuch, D., and D. S. Cherkauer (1998), Variations in hydraulic conductivity with scale of measurement during aquifer tests in heterogeneous, porous carbonate rocks, Hydrogeology Journal, 6(2), 204-215.
Sanchez-Vila, X., J. Carrera, and J. P. Girardi (1996), Scale effects in transmissivity, Journal of Hydrology, 183(1–2), 1-22.
Sanchez-Vila, X., P. M. Meier, and J. Carrera (1999), Pumping tests in heterogeneous aquifers: An analytical study of what can be obtained from their interpretation using Jacob's Method, Water Resources Research, 35(4), 943-952.
Trinchero, P., X. Sanchez-Vila, and D. Fernàndez-Garcia (2008), Point-to-point connectivity, an abstract concept or a key issue for risk assessment studies?, Advances in Water Resources, 31(12), 1742-1753.
USGS (2015), ModelMuse, US Geological Survey.
Vogel, H. J., and K. Roth (2001), Quantitative morphology and network representation of soil pore structure, Advances in Water Resources, 24(3–4), 233-242.
Western, A. W., G. Blöschl, and R. B. Grayson (2001), Toward capturing hydrologically significant connectivity in spatial patterns, Water Resources Research, 37(1), 83-97.
Willmann, M., J. Carrera, and X. Sanchez-Vila (2008), Transport upscaling in heterogeneous aquifers: What physical parameters control memory functions?, Water Resources Research, 44(12), W12437.

Xu, C., P. A. Dowd, K. V. Mardia, and R. J. Fowell (2006), A Connectivity Index for Discrete Fracture Networks, Mathematical Geology, 38(5), 611-634.
Zhou, H., J. J. Gómez-Hernández, H.-J. Hendricks Franssen, and L. Li (2011), An approach to handling non-Gaussianity of parameters and state variables in ensemble Kalman filtering, Advances in Water Resources, 34(7), 844-864.
Zinn, B., and C. F. Harvey (2003), When good statistical models of aquifer heterogeneity go bad: A comparison of flow, dispersion, and mass transfer in connected and multivariate Gaussian hydraulic conductivity fields, Water Resources Research, 39(3), 1051.

FIGURES

Figure 1. Function U representation considering one pumping well and one observation point shown by the singularities.

Figure 2. Y (=ln T) field created through a Sequential Gaussian Simulation. The inner domain (left) and the simulation domain where wells are located (right) are represented.

Figure 3. Sketch of the numerical setup representing the homogeneous outer domain (H.O.D.), the heterogeneous inner domain (H.I.D., size 20x10) and heterogeneous simulating domain (H.S.D., size 8x4). All distances are normalized by the corresponding directional variogram range (R_x and R_Y).

Figure 4. Model domain with a detailed centered random K field corresponding to the simulation domain and two well distribution configurations. Regular (left) and deliberated (right) distributions.

Figure 5. Flow connectivity between pumping and observation wells representation for regular (left) and deliberated (right) distributed wells. Green lines indicate good connectivity, and red lines are indicative of bad connectivity; line thickness are proportional to magnitude.

Figure 6. Stochastic estimation of Y fields for regular distributed wells case. (a) Reference Y map, (b) estimated by simple kriging using sampled point Y values and (d) estimated only from w' values ($l_i^Y = 0$).

Figure 7. Stochastic estimation of Y maps for deliberated distributed wells case. (b) estimated by a simple kriging using sampled point Y values , (c) estimated from sampled point Y and w' values and (d) estimated from w' values ($l_i^Y = 0$).

Figure 8. New configuration of pumping tests represented in the initial heterogeneous Y field.

Figure 9. Comparison of w' values obtained in the pumping tests realised taking into account the interpolated Y maps and the initial Y field. These corresponding quadratic

736 regression coefficient (r^2) and slope of the regression line (m) are displayed for each
737 plot.

738 **Figure 10.** Cumulative mass as a function of time for the initial *T* field, and two
739 interpolated fields obtained from kriging using 9 local *Y* values, and cokring using 9
740 local Y values and 18 available w' values (from Figure 6).

741

Figure 1.

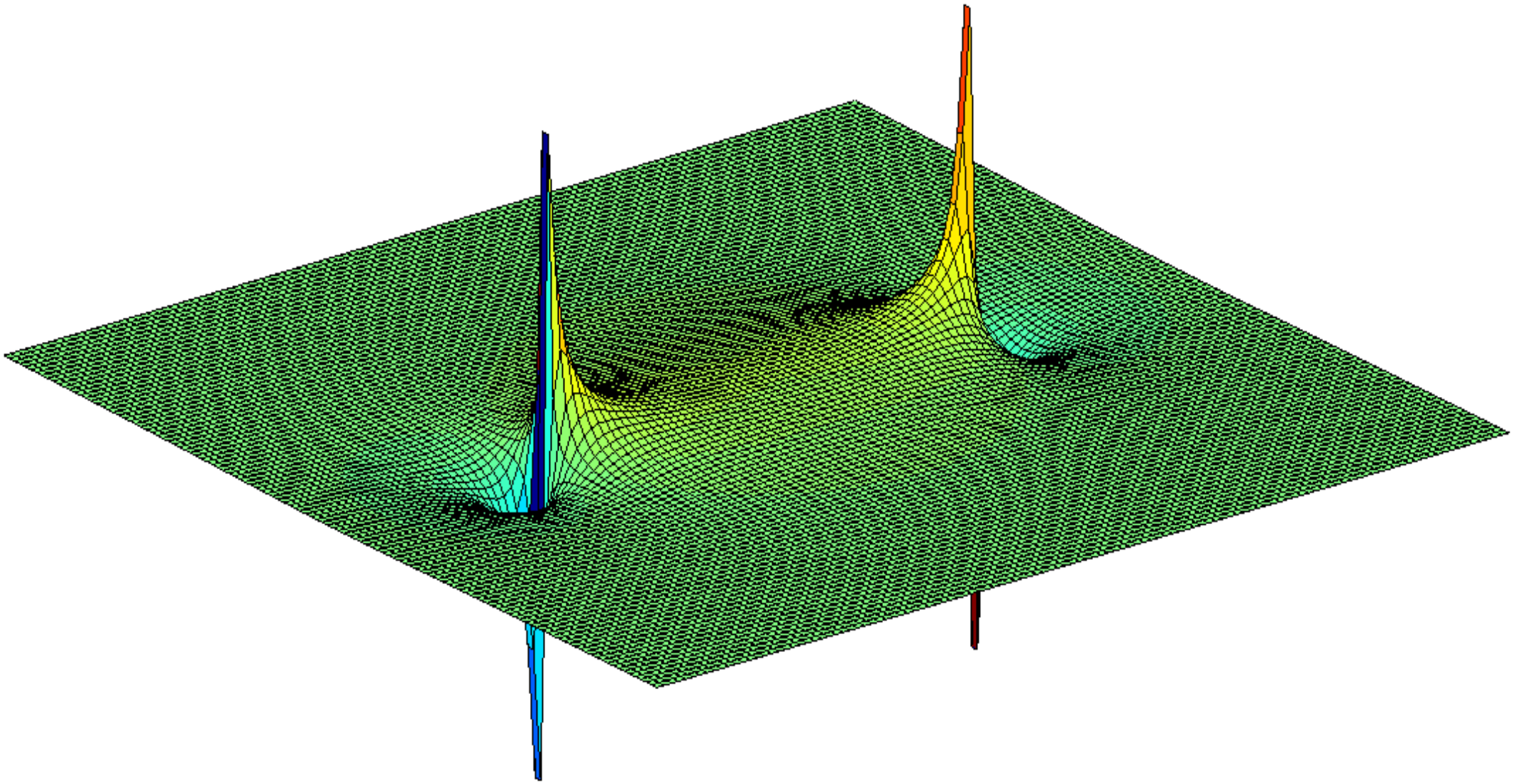

Figure 2.

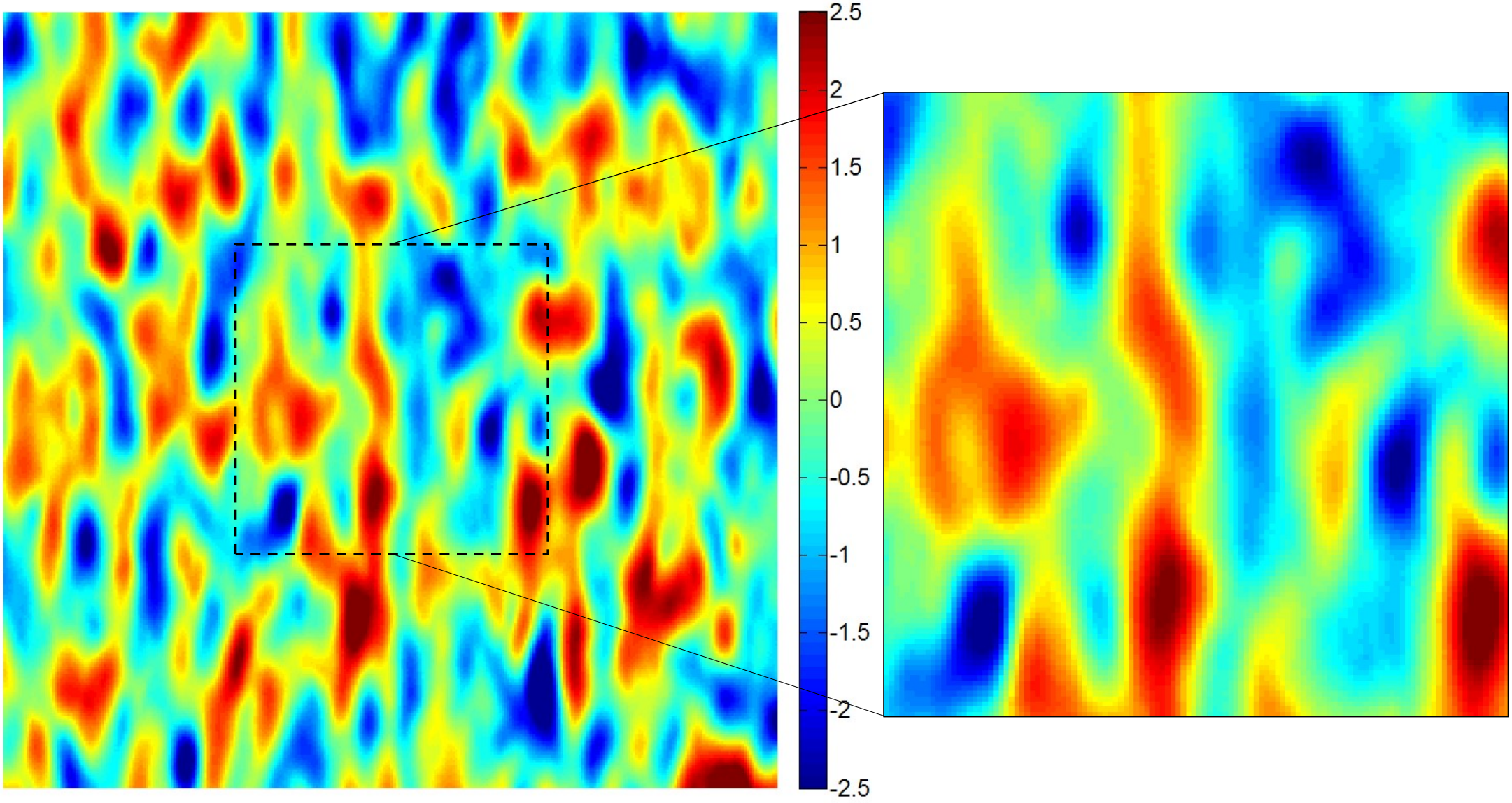
2.5
2
1.5
1
0.5
0
-0.5
-1
-1.5
-2
-2.5

Figure 3.

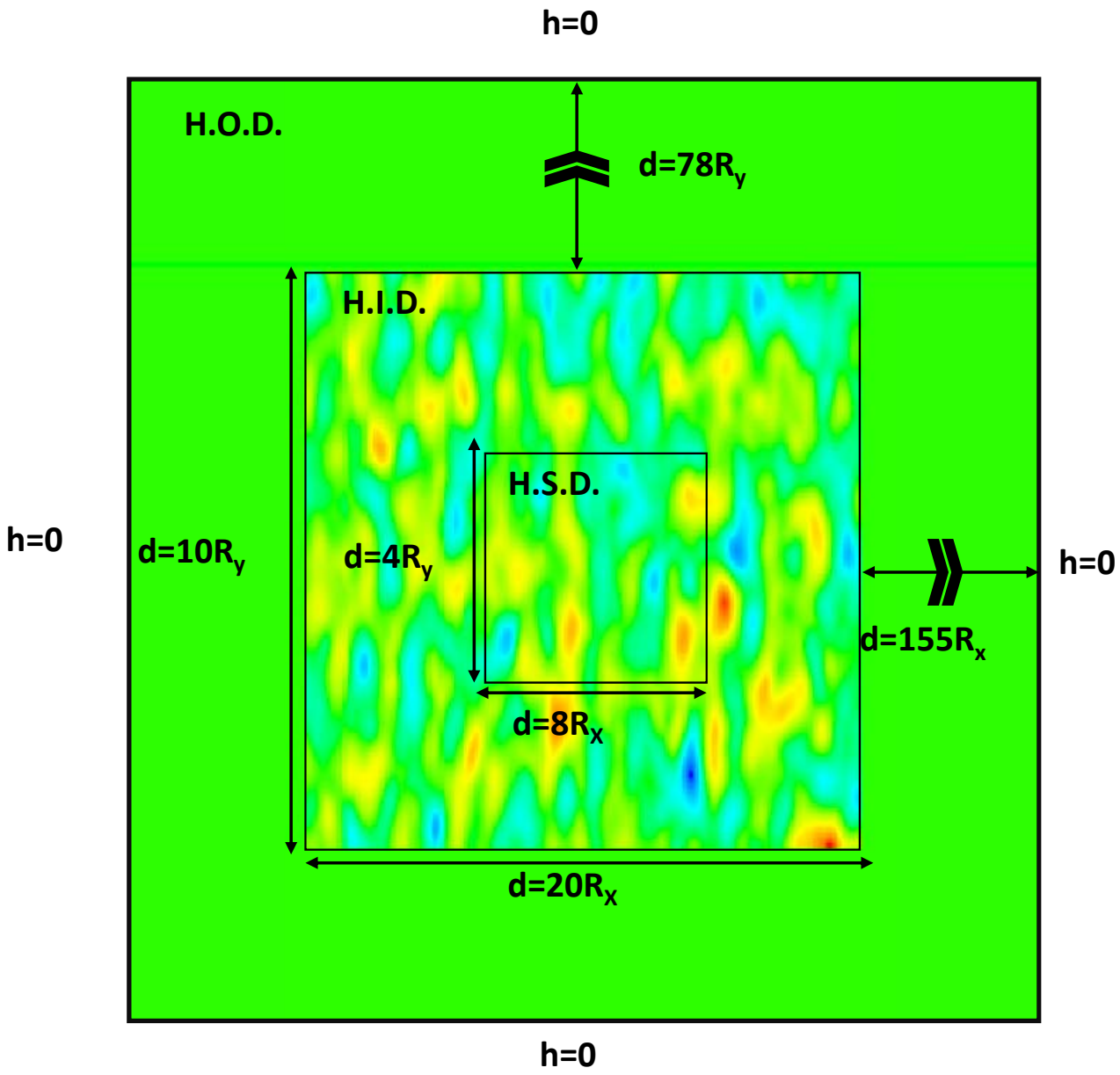
h=0
H.O.D.
d=78R_y
H.I.D.
H.S.D.
h=0
d=10R_y
d=4R_y
h=0
d=155R_x
d=8R_X
d=20R_X
h=0

Figure 4.

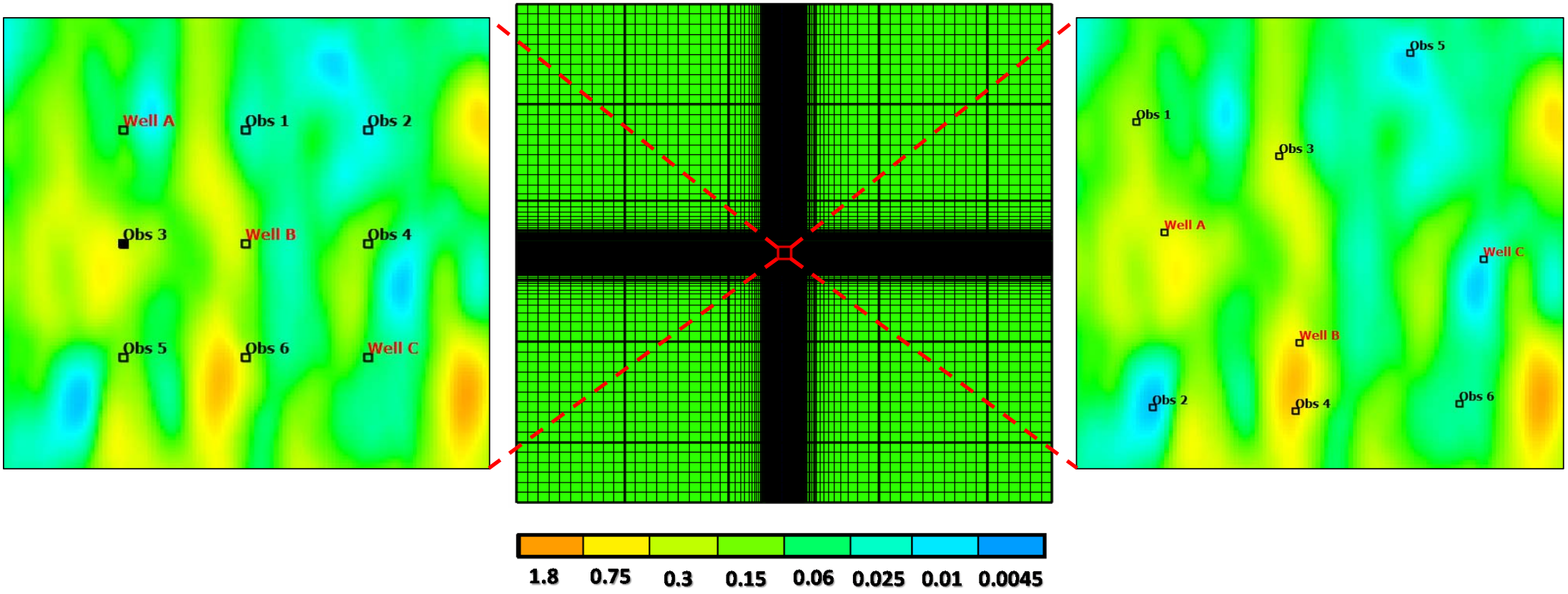
Well A
Obs 1
Obs 2
Obs 3
Well B
Obs 4
Obs 5
Obs 6
Well C
Obs 5
Obs 1
Obs 3
Well A
Well C
Well B
Obs 2
Obs 4
Obs 6
1.8
0.75
0.3
0.15
0.06
0.025
0.01
0.0045

Figure 5.

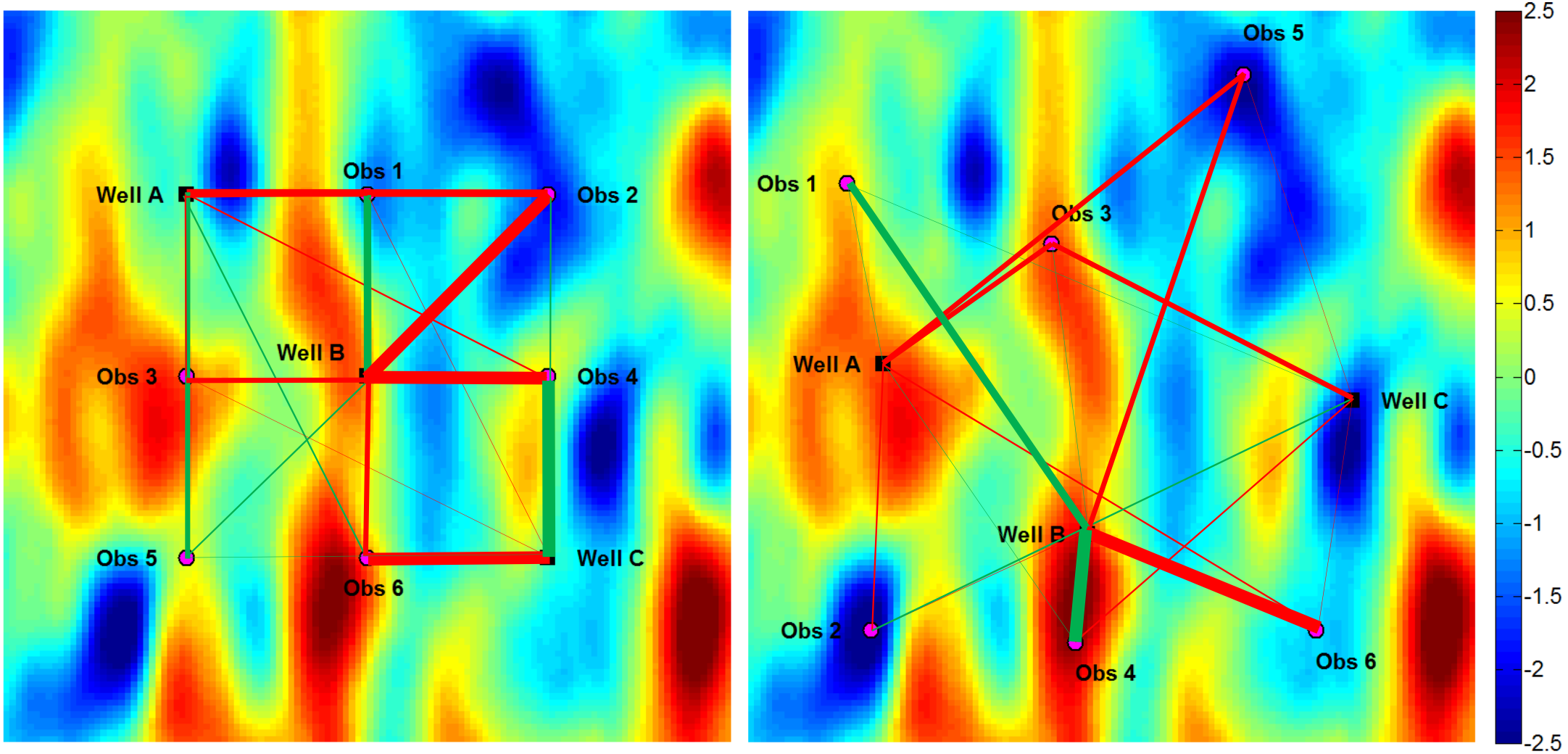
Well A
Obs 1
Obs 2
Well B
Obs 3
Obs 4
Obs 5
Obs 6
Well C
Obs 1
Obs 5
Obs 3
Well A
Well C
Well B
Obs 2
Obs 4
Obs 6
2.5
2
1.5
1
0.5
0
-0.5
-1
-1.5
-2
-2.5

Figure 6.

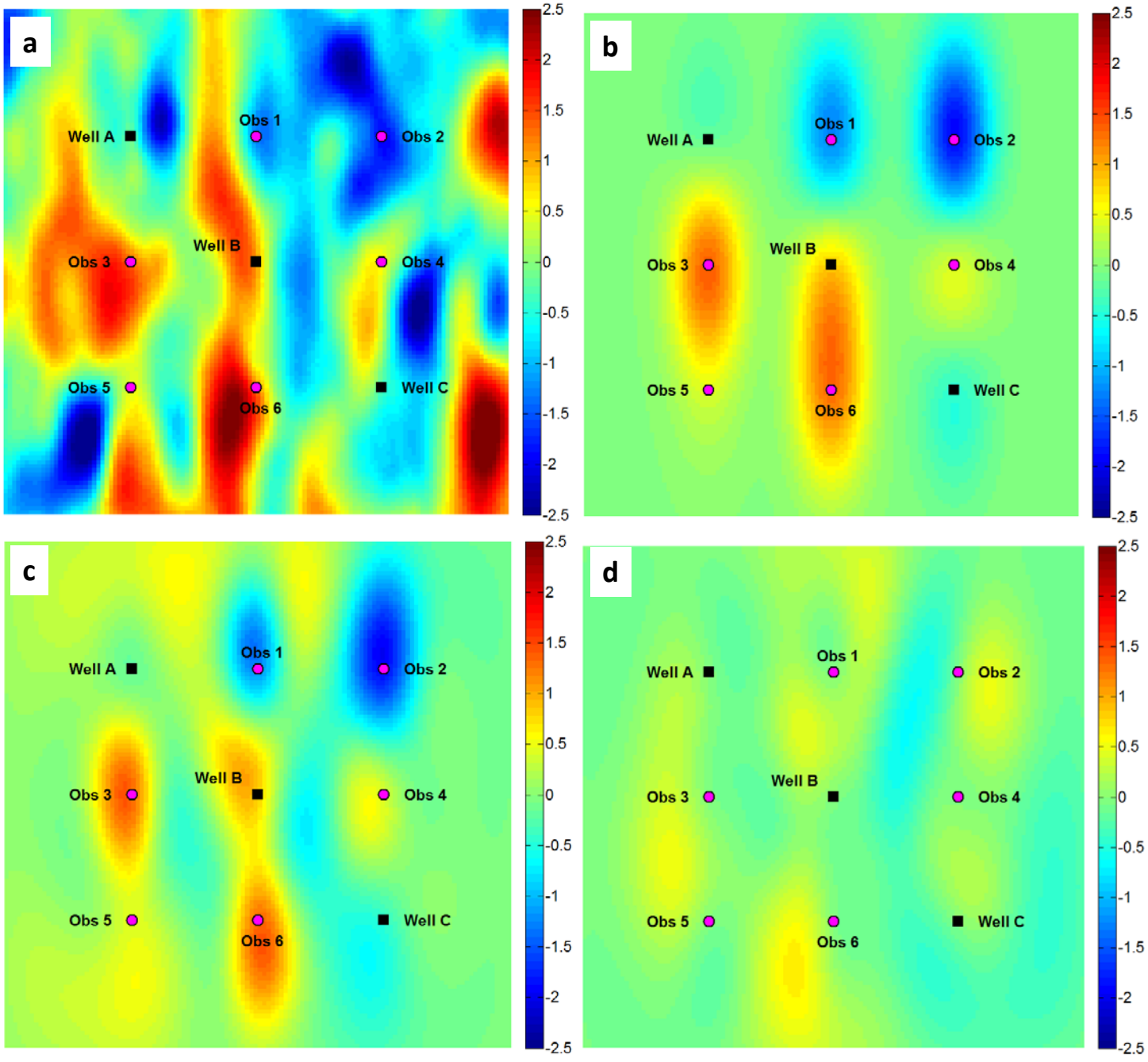
a
Well A
Obs 1
Obs 2
Obs 3
Well B
Obs 4
Obs 5
Obs 6
Well C
2.5
2
1.5
1
0.5
0
-0.5
-1
-1.5
-2
-2.5
b
Well A
Obs 1
Obs 2
Obs 3
Well B
Obs 4
Obs 5
Obs 6
Well C
2.5
2
1.5
1
0.5
0
-0.5
-1
-1.5
-2
-2.5
c
Well A
Obs 1
Obs 2
Obs 3
Well B
Obs 4
Obs 5
Obs 6
Well C
2.5
2
1.5
1
0.5
0
-0.5
-1
-1.5
-2
-2.5
d
Well A
Obs 1
Obs 2
Obs 3
Well B
Obs 4
Obs 5
Obs 6
Well C
2.5
2
1.5
1
0.5
0
-0.5
-1
-1.5
-2
-2.5

Figure 7.

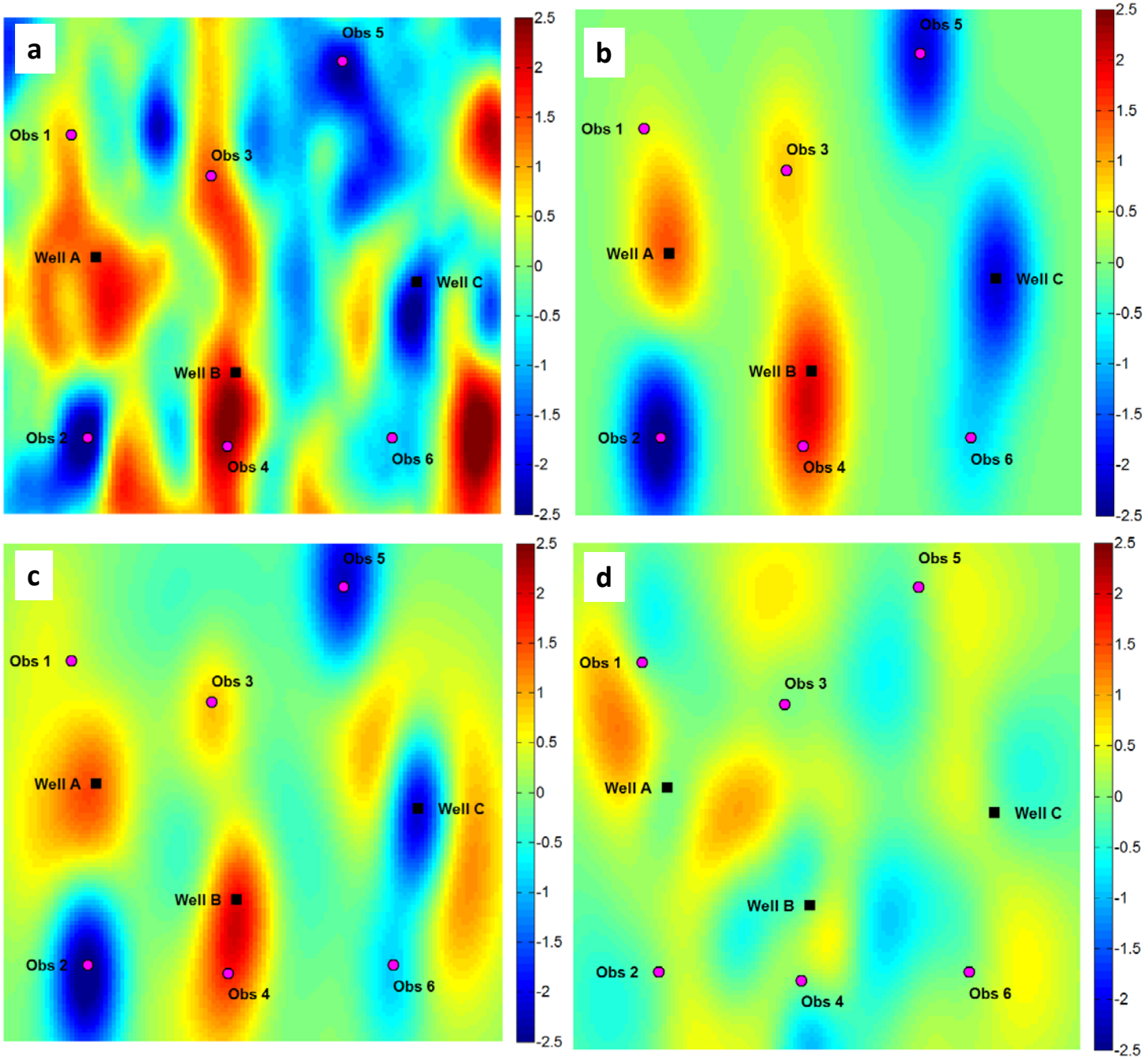
a
Obs 5
Obs 1
Obs 3
Well A
Well C
Well B
Obs 2
Obs 4
Obs 6
2.5
2
1.5
1
0.5
0
-0.5
-1
-1.5
-2
-2.5
b
Obs 5
Obs 1
Obs 3
Well A
Well C
Well B
Obs 2
Obs 4
Obs 6
2.5
2
1.5
1
0.5
0
-0.5
-1
-1.5
-2
-2.5
c
Obs 5
Obs 1
Obs 3
Well A
Well C
Well B
Obs 2
Obs 4
Obs 6
2.5
2
1.5
1
0.5
0
-0.5
-1
-1.5
-2
-2.5
d
Obs 5
Obs 1
Obs 3
Well A
Well C
Well B
Obs 2
Obs 4
Obs 6
2.5
2
1.5
1
0.5
0
-0.5
-1
-1.5
-2
-2.5

Figure 8.

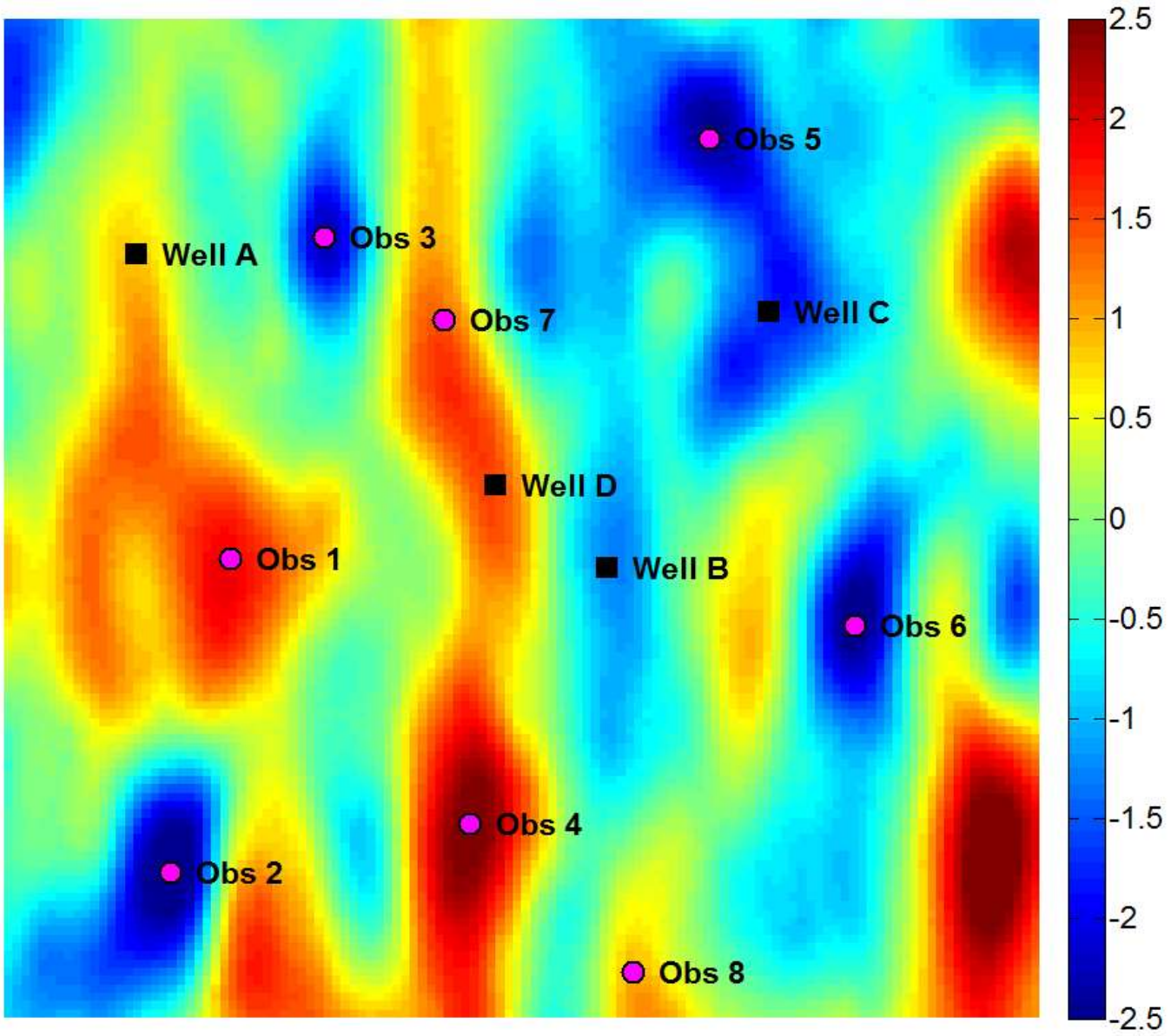
Obs 5
Obs 3
Well A
Obs 7
Well C
Well D
Obs 1
Well B
Obs 6
Obs 4
Obs 2
Obs 8
2.5
2
1.5
1
0.5
0
-0.5
-1
-1.5
-2
-2.5

Figure 9.

Regular distributed wells

Deliberated distributed wells

(a)

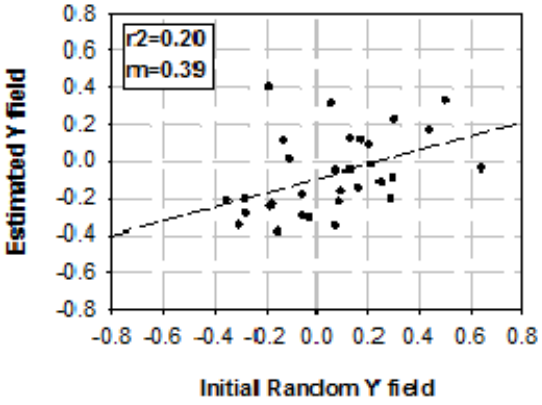

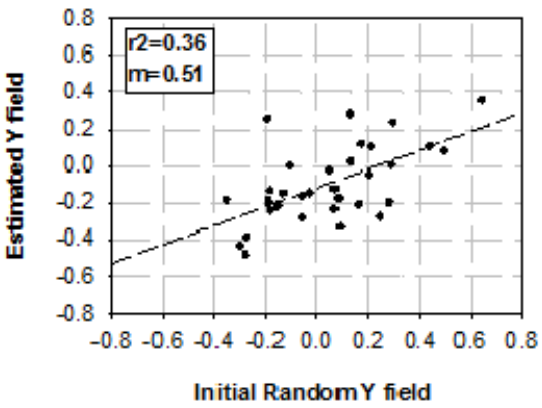

(a)

(b)

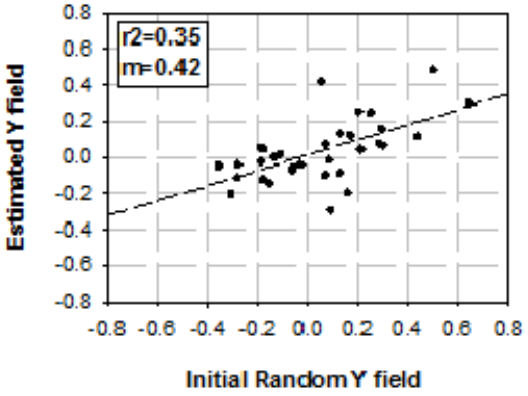

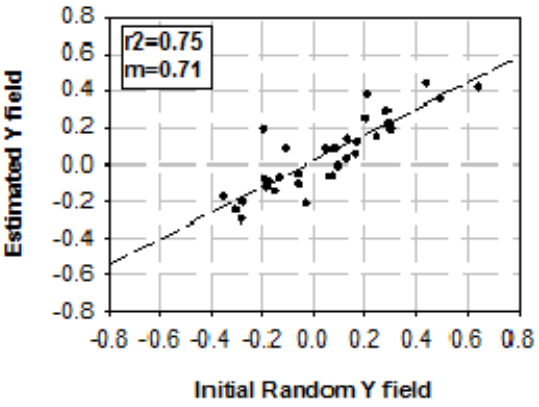

(b)

(c)

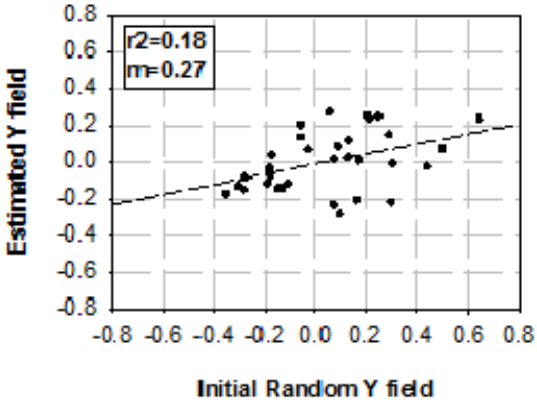

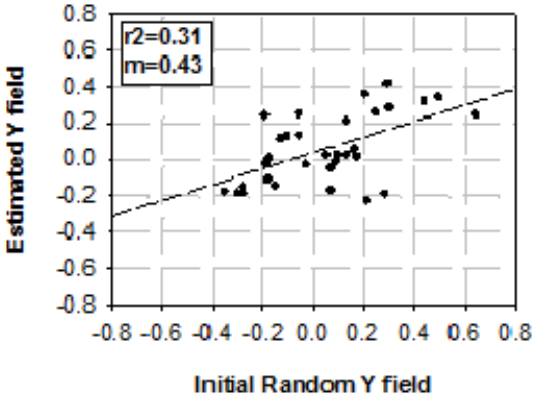

(c)

Figure 10.

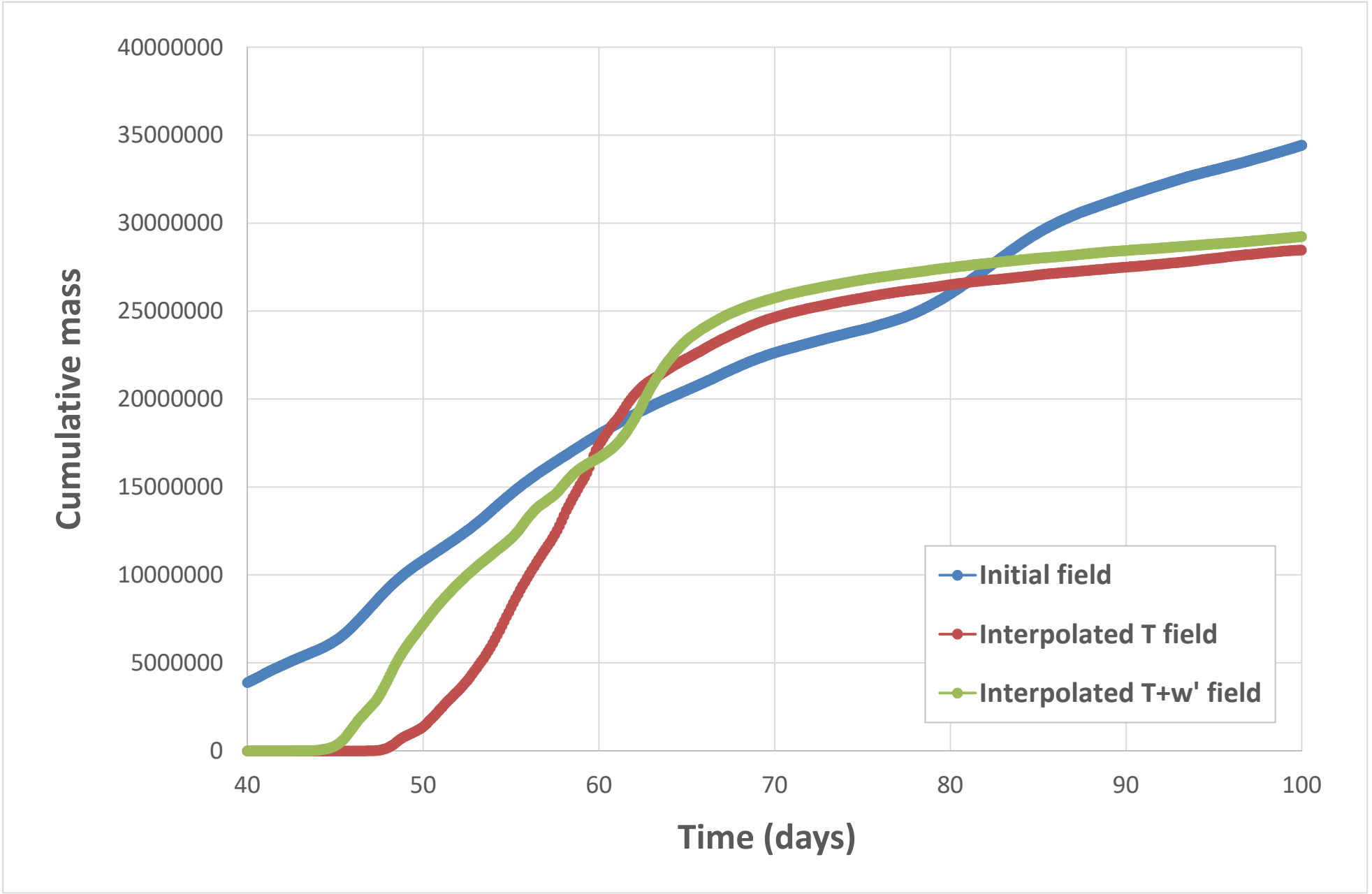
40000000
35000000
30000000
25000000
20000000
15000000
10000000
5000000
0
Cumulative mass
40
50
60
70
80
90
100
Time (days)
Initial field
Interpolated T field
Interpolated T+w' field